



Full Text View

[Volume 28, Issue 5 \(May 1998\)](#)

Journal of Physical Oceanography

Article: pp. 971–983 | [Abstract](#) | [PDF \(201K\)](#)

Simple Models of Flow over Deep Ocean Sills: Planetary and Semigeostrophic Solutions

David N. Straub*

Atmospheric and Oceanic Sciences, McGill University Montreal, Quebec, Canada

(Manuscript received September 5, 1995, in final form September 12, 1997)

DOI: 10.1175/1520-0485(1998)028<0971:SMOFOD>2.0.CO;2

ABSTRACT

Simple inverted reduced-gravity models of flow over deep ocean sills are considered, with emphasis placed on the case for which sills are wide with respect to the abyssal Rossby radius. When the length scale of the flow is also large compared to the Rossby radius, an f -plane version of the planetary geostrophic (PG) equations applies. These equations, however, predict a collapse in scale of the flow so that the PG approximation breaks down and higher-order dynamics must be evoked. Whether or not the collapsing PG dynamics give way to semigeostrophy (SG) or to some other balance regime is also discussed.

Next, the steady semigeostrophic equations typically used in rotating hydraulics studies are considered. For relatively wide sills, as well as for narrow sills that are not elongated, the path taken by the overflow is not well constrained by the sill geometry alone. The collapsing PG problem, however, suggests that the appropriate axis of flow follows a branch of the separatrix isobath. Also suggested by the PG dynamics is that there may be a mass of quiescent water adjacent to the overflow current. Dependence of the maximum flux across the sill on assumptions regarding the flow path and the presence or absence of a quiescent water mass are therefore considered. These are compared with dependencies on sill width and the potential vorticity of the overflow. Finally, flow upstream and downstream of the sill is considered. In particular, a case in which multiple equilibria exist downstream of the sill is discussed.

Table of Contents:

- [Introduction](#)
- [Wide sills and “f-plane](#)
- [Steady semigeostrophic](#)
- [Conditions upstream and](#)
- [Summary](#)
- [REFERENCES](#)
- [FIGURES](#)

Options:

- [Create Reference](#)
- [Email this Article](#)
- [Add to MyArchive](#)
- [Search AMS Glossary](#)

Search CrossRef for:

- [Articles Citing This Article](#)

Search Google Scholar for:

- [David N. Straub](#)

1. Introduction

The effects of sill geometries on the outflows of dense water spilling over deep ocean sills is thought to be of importance

to the properties and amounts of water feeding the ocean's thermohaline circulation. Although entrainment, dissipation, and transient effects are clearly important to any complete picture of these flows, the steady inviscid problem has also attracted much interest. This problem has traditionally been addressed from the perspective of rotating hydraulics (e.g., [Stern 1972](#); [Whitehead et al. 1974](#); [Gill 1977](#)). The simplest case considers a single reduced-gravity layer and takes the geometry of the channel to have a rectangular cross section, so that the channel depth varies only with the alongchannel coordinate (see [Pratt and Lundberg 1991](#) for a review). Sills having nonrectangular cross sections have also been considered (e.g., [Borenas and Lundberg 1986](#); [Killworth 1992](#); [Dalziel 1992](#)) as have effects relating to the flow having a more complex baroclinic structure (e.g., [Pratt and Armi 1990](#)).

It is generally assumed that the main axis of the flow is known and that the component of flow parallel to this axis is geostrophic. The across-stream component of flow is taken to be fully nonlinear so that semigeostrophic (SG) dynamics apply. These assumptions are clearly valid for narrow elongated sills. Many deep ocean sills, however, cannot be considered narrow in the sense that they are wide compared to the abyssal Rossby radius. For example, the Ceara Abyssal Plain, the Vema Channel, Iceland–Faeroe Passage, and Samoa Passage are all examples of wide sills. Additionally, some sills, such as the Iceland–Faeroe Passage, are not elongated (i.e., longer than they are wide). Thus, it is not immediately obvious that SG dynamics are appropriate for describing flow over many deep ocean sills. In particular, unless the flow develops length scales comparable to the Rossby radius, the across-stream flow need not be ageostrophic. Furthermore, if the current does become narrow, then the main axis of the flow need not correspond to that of the sill.

On the other hand, assuming the flow across a wide sill to be semigeostrophic can lead to solutions having current widths on the order of the Rossby radius. That is, assuming SG leads to solutions consistent with the assumptions inherent to the semigeostrophic approximation. For example, Killworth ([Killworth 1994](#), hereafter K94) treats the case of flow across wide simple sills. His analysis allows for a mass of stagnant water to exist adjacent to the overflow current, this being motivated by numerical integrations of the shallow-water equations. The across-sill transport was maximized in the limit of vanishing potential vorticity, for which the width of the current was comparable to the Rossby radius.

The present work addresses unidirectional flow for a reduced gravity layer of fluid. Emphasis is placed on wide sills and on sills that are not elongated. The paper is organized as follows. [Section 2](#) considers a case in which the length scale of the flow is, at least initially, large compared to the Rossby radius. This leads to a well known f -plane analog to the planetary geostrophic (PG) equations. The dynamics are similar to those assumed recently by [Salmon \(1995\)](#) to model flow in the Samoa Passage. The PG dynamics predicts a flow that collapses into a narrow jet and, as this happens, higher-order effects must be invoked. Nevertheless, the PG problem suggests several aspects of the full solution that seem to be robust to how the collapse is arrested (e.g., whether by invoking friction or by nonlinearities). For example, the stagnant water mass assumption of K94 results naturally from the collapse. Additionally, the PG dynamics appear to determine the across-sill transport and to confine the overflow current to lie on a branch of the separatrix isobath—that is, along an isobath containing the deepest point on the sill. It is also pointed out that the PG solution bares at least a qualitative resemblance to observations that have led to the suspicion that flow across deep ocean sills may be hydraulically controlled. Finally, because SG dynamics are typically used to model flow over sills, the question of whether the collapsing PG dynamics gives way to SG is also addressed.

[Section 3](#) considers the steady SG problem for moderately wide and narrow sills. The focus is on how the maximal across-sill transport depends on the following: the presence or absence of a stagnant water mass adjacent to the flow, the sill width, the potential vorticity of the overflow current, and the angle at which the flow is assumed to cross the sill. It is found that for wide sills the transport is generally insensitive to all of these factors, except for the presence of the stagnant water mass. For narrow sills that are not elongated, the allowed transport can be sensitive to the angle at which the flow crosses the sill.

[Section 4](#) considers conditions upstream and downstream of the sill, still assuming SG dynamics. It is argued that, typically, fluid on one side of the overflow current flows uphill as it crosses the sill, whereas fluid on the other side flows downhill. An exception to this is the case of sills with rectangular cross sections, for which all columns must flow first uphill and then downhill as they cross the sill. Finally, an example is given in which there exist multiple equilibria downstream of the sill. Since the two equilibria are physically close to one another, it is speculated that they might correspond to the far-field solutions of a rotating hydraulic jump. The nature of this hypothesized jump is compared with the rotating hydraulic jump found by Pratt (1986).

A brief summary is offered in [section 5](#).

2. Wide sills and “ f -plane planetary geostrophic” dynamics

This section considers an f -plane analog to planetary geostrophic dynamics for a reduced gravity layer of fluid. [Section 2a](#) derives the basic equations and considers a PG analog to the “dam break” problem. It is found that a flow that is initially consistent with the PG approximation evolves into one that is not. The nature of the collapse of the PG dynamics is

discussed in [section 2b](#).

a. Basic equations and steady solution

Consider a flow over a wide sill in an abyssal layer of uniform density. Overlying this abyssal layer is a thick layer of less dense water that is taken to be at rest. Furthermore it is assumed that, at least initially, the horizontal length scale of the flow is sufficiently large so that the Rossby number, $Ro \doteq U/fL$, can be considered small. Here U and L are the horizontal velocity and length scales of the flow and f is the Coriolis parameter. It is also assumed that the flow evolves slowly. That is, δ must also be small, where $\delta \doteq 1/fT$ and T is the timescale of the flow evolution. The horizontal velocity is thus in geostrophic balance:

$$f\mathbf{u} = g'\mathbf{k} \times \nabla\eta + O(Ro, \delta), (1)$$

where g' is the reduced gravity and η gives the height of the interface above the deepest point on the sill. The Coriolis parameter is taken to be constant and the leading-order flow is thus horizontally nondivergent. If topographic variations were also taken to be small, then the leading-order equations would be degenerate. When $O(1)$ variations in topography are allowed, however, it is straightforward to close the system without going to higher order. The resulting equation is an f -plane analog to the PG interface height field equation for a reduced gravity layer of fluid.

The leading-order potential vorticity (or interface height field) equation is formed by substituting [\(1\)](#) into the continuity equation

$$\eta_t + \nabla \cdot [(\eta - h)\mathbf{u}] = 0 (2)$$

to get

$$\eta_t - \frac{g'}{f} J(\eta, h) = 0. \quad (3)$$

Here $(\eta - h)$ is the thickness of the layer and $J(a, b) \doteq a_x b_y - b_x a_y$. [Equation \(3\)](#) can be thought of as a potential vorticity equation in which the layer thickness plays the role of potential vorticity. It can also be written as

$$\eta_t + \mathbf{c} \cdot \nabla \eta = 0, (4)$$


where

$$\mathbf{c} \doteq \frac{g'}{f} (\mathbf{k} \times \nabla h). \quad (5)$$

[Equations \(4\), \(5\)](#) describe a system in which information propagates along characteristics, which here are coincident with isobaths. The sense of the propagation is such that deeper topography lies to the left for positive f . Note that the characteristic velocity, \mathbf{c} , is unidirectional in the sense that its direction is uniquely defined at each point for which ∇h is nonzero. This distinguishes the dynamics here from those of rotating hydraulics for which gravity waves can potentially propagate both upstream and downstream.

For generic sill topographies, there will generally be one or more saddle points in h , and \mathbf{c} vanishes at these points. Except in special cases, there will be a deepest saddle point lying along the sill. In the interest of simplicity, it is assumed that this is the only saddle in the depth range of interest. Also for convenience, the value of h at this point is chosen to be zero, with negative values corresponding to deeper topography. Near the saddle point, h is approximated by

$$h(x, y) \approx A(x^2 - \alpha^2 y^2). (6)$$

Thus, close to the saddle point, topography shoals parabolically with x and deepens parabolically with y . [Figure 1](#) 

We consider a PG analog to the classic ‘‘dam break’’ problem ([Gill 1976](#)). Initial conditions are as follows. Far upstream (say for $y \geq y_0$) the abyssal layer is filled above the level of the sill to an ambient level $\eta = \eta_0$. Far downstream of the sill (say for $y \leq -y_0$) the abyssal layer is filled to an ambient level, $\eta = \eta_1$, where $\eta_1 < 0$. Between y_0 and $-y_0$, η varies smoothly from η_0 to η_1 . The Rossby adjustment is assumed to have already taken place so that the PG approximation is

valid, at least initially, provided $y_0 \gg L_{Ro}$, where L_{Ro} is an appropriately defined Rossby radius (e.g., $L_{Ro} \doteq (g'\eta_0)^{1/2}/f$).

The long time solution shows that the PG approximation must eventually break down. From (4), (5), the long time solution at a particular point is given by the initial value of η far “upstream” in the characteristic velocity sense. Referring to Fig. 1, points such that $\alpha y > x$ (i.e., the upper left-hand half of the figure) lie on characteristics that extend back to large positive y . Hence, the long time solution in this region is given by the initial condition far upstream. Thus, η takes on a value of η_0 in this region. Conversely, points on the lower right-hand side of Fig. 1 all lie on characteristics that extend back to $y < -y_0$. In this region the steady solution is such that the abyssal layer is filled to a level $z = \eta_1$. On isobaths lying above the horizontal surface, $z = \eta_1$, the abyssal layer is empty at $t = \infty$.

Thus, the solution becomes discontinuous. To see how the discontinuity develops, note first from (4), (5) that $\mathbf{c} = 0$ at the saddle so that η remains constant. However, at a point just upstream of the saddle [e.g., $(x, y) = (0, y_1)$, where $0 < y_1 < y_0$], η eventually takes on the value η_0 . The time necessary for η to take on its steady-state value at this point is the travel time t from $y = y_0$ to $y = y_1$, moving at the characteristic velocity, \mathbf{c} . For example, if point B in Fig. 1 corresponds to $(0, y_1)$, then t is the travel time from A to B, moving at speed $|\mathbf{c}|$. Solving for t then amounts to doing a line integral along the isobath connecting A to B:

$$t(y_1) = \int_0^{\lambda} \frac{d\lambda'}{|\mathbf{c}|}, \quad (7)$$

where λ is the distance from A. Using (4)–(6), one gets, after a bit of algebra, that

$$t(y_1) = \frac{f}{2g'A\alpha} \ln \left[\frac{y_1}{y_0 - (y_0^2 - y_1^2)^{1/2}} \right]. \quad (8)$$

Inverting for y_1 then gives a characteristic length scale of the solution as a function of time:

$$y_1(t) = \frac{2y_0 e^{\sigma t}}{1 + e^{2\sigma t}}, \quad (9)$$

where $\sigma \doteq 2g'A\alpha/f$. With increasing time, $y_1 \rightarrow 0$ and the PG approximation breaks down.

The discontinuity is not limited to the saddle point but extends outward from the saddle along that branch of the separatrix for which \mathbf{c} is directed away from the saddle (i.e., along the line $\alpha y = x$). To see this, consider the long time solution on either side of the separatrix near points C and D in Fig. 1. Near C, a point lying on an isobath slightly shallower than the separatrix is on a characteristic that extends back to $y = -\infty$. Hence, the long time solution at this point will correspond to the initial condition at $y = -\infty$ on this isobath. Assuming the isobath to lie above the ambient level to which the downstream basin is filled (i.e., above $z = \eta_1$), the abyssal layer becomes empty here. Conversely, just to the left of C, topography is slightly deeper than the separatrix isobath and characteristics extend back to $y = +\infty$. Hence, on this side of the separatrix, the long time solution is given by $\eta = \eta_0$. Therefore, the solution becomes discontinuous at C. Similar arguments show that the same is true at point D. Thus, the PG solution collapses to a narrow jet lying along the line $\alpha y = x$. The transport carried by the jet is

$$T_0 = \frac{g'}{2f} \eta_0^2, \quad (10)$$

and the sense of the flow is from C to D.

A similar narrowing of a current with time (until nonlinear or diffusive effects become important) is described in the related problem of Rossby adjustment over a step (e.g., Gill et al. 1986; Johnson 1985). Differences are that here topographic Rossby waves play the role of the double Kelvin waves in the step problem and also the interface height field grounds.

Assuming that the discontinuity can be mended either by friction or by nonlinearities, we interpret the PG solution as

suggesting that the overflow current will have the two following properties:

1. It will be sufficiently narrow such that the PG approximation breaks down.
2. It will be constrained to lie roughly parallel to the separatrix isobath.

It is interesting to note that the details of how the discontinuity is mended has only a minimal impact on the predicted transport across the sill, provided that the alongstream component of flow remains geostrophic. Taking n to be a coordinate perpendicular to the axis of the current, the geostrophic transport (directed from C to D) is given by

$$\begin{aligned} T &= \frac{-g'}{f} \int_{n_0}^{n_1} (\eta - h) \frac{\partial \eta}{\partial n} dn \\ &= T_0 + \frac{g'}{f} \int_{n_0}^{n_1} h \frac{\partial \eta}{\partial n} dn + \mathcal{O}(\epsilon^2), \end{aligned} \quad (11)$$

where $\epsilon \doteq h_0/\eta_0$. Here h_0 is the value of h where the interface height field grounds and n_0 and n_1 are defined such that $\eta = \eta_0$ at $n = n_0$ and $\eta = h_0$ at $n = n_1$. Scaling $|\eta_n|$ like $\eta_0/(n_1 - n_0)$ then gives that

$$T = T_0 - \mathcal{O}\left(\frac{g'h_0\eta_0}{f}\right) = T_0[1 - \mathcal{O}(\epsilon)]. \quad (12)$$

Near the saddle point, h_0 scales like the curvature of the topographic height field multiplied by the square of the current width. That is, using (6), $h_0 \sim \mathcal{O}(AL^2)$. Thus, if the transport is assumed to be constrained at the saddle, then any closure of the PG problem yielding an L such that $AL^2 \ll \eta_0$ will give essentially the same across sill transport.

It is also of interest to note a qualitative resemblance in the structure of the density field between the PG solution and the case of nonrotating hydraulically controlled flow over a sill. A resemblance between the latter of these and observations has led to the suspicion that flow across deep ocean sills may be hydraulically controlled (e.g., [Whitehead 1995](#)). [Figure 2](#) compares the long time solution for η in the PG problem with a schematic depicting the height of an isopycnal surface for the case of nonrotating classical control. The behavior is qualitatively similar. That is, in both cases there is a sharp gradient in the interface height field across the sill. Of course, in the PG case, this gradient is infinite. Addition of a modest amount of bottom friction to the problem, however, would be enough to smooth out this discontinuity. Furthermore, this would allow for a bottom Ekman layer to develop, which could prevent the interface from grounding in the PG problem. That is, bottom friction would tend to increase the resemblance between, say, the profiles in [Figs. 2b and 2c](#). In this sense, the PG dynamics predicts a density field that is at least qualitatively similar to the observations that have led to the supposition that flow over deep sills may be hydraulically controlled.

b. Nature of the collapse

In this subsection, we ask whether the collapsing PG system gives way to SG or to some other balanced regime. To answer this question, we must see which of the underlying assumptions of the PG equations gives way first as the width of the current decreases. These assumptions are threefold: that δ remain small, that Ro remain small, and that the $\mathcal{O}(\text{Ro}, \delta)$ corrections to the geostrophic velocity remain negligible in the mass continuity equation. The steady SG dynamics typically used to describe flow over sills assumes that the Rossby number and the ageostrophic terms in the continuity equation are both $\mathcal{O}(1)$. Below, we find that the latter of these become important while the Rossby number is still a small parameter. That is, the PG dynamics gives way to a geostrophic regime that is similar to an intermediate geostrophic regime described elsewhere in the literature (e.g., [Williams and Yamagata 1984](#), hereafter WY84; [Cushman-Roisin 1986](#), hereafter C86). The regime found here is essentially an f -plane version of the frontal geostrophic dynamics described in those papers.

To get a clear idea of how the PG system breaks down, it is helpful to nondimensionalize the equations of motion. To do this, we use the quantities L and T already introduced and take η_0 as a vertical scale—that is, we take $(\eta - h)$ to scale like η_0 . Finally, the velocity scale U is taken to obey geostrophic scaling, $fUL = g'\eta_0$. Then, the nondimensionalized momentum equation becomes

$$\delta \mathbf{u} + \text{Ro}(\mathbf{u} \cdot \nabla \mathbf{u}) + \mathbf{k} \times \mathbf{u} = -\nabla \eta. \quad (13)$$

We proceed by assuming Ro and δ to be small so that \mathbf{u} may be replaced by its geostrophic approximation, \mathbf{u}_g , in the $O(Ro, \delta)$ terms above. That is,

$$\begin{aligned} \delta \frac{\partial \mathbf{u}_g}{\partial t} + Ro(\mathbf{u}_g \cdot \nabla \mathbf{u}_g) + \mathbf{k} \times \mathbf{u} \\ = -\nabla \eta + O(Ro^2, \delta Ro, \delta^2). \end{aligned} \quad (14)$$

Solving for \mathbf{u} then gives

$$\mathbf{u} \approx \mathbf{u}_g + Ro \mathbf{u}_1 + \delta \mathbf{u}_2, \quad (15)$$

where

$$\mathbf{u}_1 \doteq (\mathbf{k} \times \mathbf{u}_g \cdot \nabla \mathbf{u}_g) \quad (16)$$

and

$$\mathbf{u}_2 \doteq \left(\mathbf{k} \times \frac{\partial \mathbf{u}_g}{\partial t} \right). \quad (17)$$

We next substitute the $O(Ro)$ and $O(\delta)$ corrections to \mathbf{u} back into the mass continuity [equation \(2\)](#). The result is written below in nondimensional form:

$$\begin{aligned} (\eta_0/T)(\eta_t + \mathbf{u}_g \cdot \nabla h) &= -Ro(\eta_0 U/L)(\eta - h)(\nabla \cdot \mathbf{u}_1) \\ &\quad - Ro(\eta_0 U/L) \mathbf{u}_1 \cdot \nabla \eta \\ &\quad - \delta(\eta_0 U/L)(\eta - h)(\nabla \cdot \mathbf{u}_2) \\ &\quad - \delta(\eta_0 U/L) \mathbf{u}_2 \cdot \nabla \eta. \end{aligned} \quad (18)$$

The terms on the lhs of [\(18\)](#) are identical to those kept in the PG system and thus will necessarily be of the same order until the PG equations break down. After this, a more careful scaling of the $\mathbf{u}_g \cdot \nabla h$ term (taking into account the developing anisotropy of the flow) would be necessary to describe the subsequent evolution. The question addressed here is which, if any, of the terms on the rhs of [\(18\)](#) become $O(1)$ before the flow becomes ageostrophic to leading order. Dividing through by $f\eta_0$ puts [\(18\)](#) into a nicer form:

$$\begin{aligned} \delta(\eta_t + \mathbf{u}_g \cdot \nabla h) + Ro^2(\eta - h)(\nabla \cdot \mathbf{u}_1) + Ro^2 \mathbf{u}_1 \cdot \nabla \eta \\ + Ro\delta(\eta - h)(\nabla \cdot \mathbf{u}_2) + Ro\delta \mathbf{u}_2 \cdot \nabla \eta = 0. \end{aligned} \quad (19)$$

From [\(19\)](#), we see that the terms on the second line are $O(Ro)$ with respect to those on the first line. Thus, as long as the Rossby number remains small, terms on the second line of [\(19\)](#) may be neglected. On the other hand, the $O(Ro^2)$ terms can enter the leading order balance if δ approaches Ro^2 .

We can thus sum up the necessary conditions for validity of the PG regime as follows. It is required that

$$Ro^2 \ll \delta \ll 1. \quad (20)$$

Thus there are two ways in which the PG dynamics could break down: either the problem develops fast timescales or the Rossby number approaches $\delta^{1/2}$. For the problem considered in [section 2a](#), however, the assumption of a small δ improves with time. For example, consider [Eq. \(8\)](#). As the current narrows, the relevant y_1 becomes small. Assuming $y_1 \ll y_0$ then gives that $t(y_1) \sim \ln(2y_0/y_1)$. In other words, the timescale of the solution goes to infinity as the log of the inverse current width. As this happens, δ decreases toward zero. Therefore, we expect the assumption of small δ to remain valid so that the PG approximation breaks down when

$$\text{Ro}^2 \sim \delta \ll 1. (21)$$

Once this condition is met, it is not clear that the current should continue to narrow with time until the flow eventually becomes semigeostrophic or if the flow might approach a steady state in an intermediate regime similar to that described in C86 and in WY84. Nevertheless, SG dynamics are often used to describe flow over deep ocean sills. This seems justified for narrow elongated sills, but is not obviously appropriate for very wide sills. The next section considers steady SG sills that are narrow to moderately wide and that are not necessarily elongated.

3. Steady semigeostrophic solutions

This section considers steady flow across sills for the case of semigeostrophic dynamics. In [section 3a](#), the basic equations of semigeostrophy are reviewed and nondimensionalized. [Section 3b](#) then considers how the flux across the sill depends on various factors.

a. Basic equations

Under steady semigeostrophic dynamics, the alongstream (l) momentum equation keeps the advective terms and the alongstream velocity is taken to be geostrophic:


$$-f\nu = -g'\eta_n \quad (22)$$

$$\mu\nu_n + \nu\nu_l + f\mu = -g'\eta_l. \quad (23)$$

Here, curvature in the flow path is ignored, n and l are the across- and alongstream coordinates respectively, and μ and ν are the corresponding velocities. The coordinates n and l form a right-handed coordinate system with l increasing upstream. They are related to x and y by

$$n = x \cos\theta - y \sin\theta \quad (24)$$

$$l = x \sin\theta + y \cos\theta, \quad (25)$$

where θ gives the angle between the y axis and the axis of flow (see [Fig. 3](#) ). For a flow path oriented along the separatrix contour and topography described by [\(6\)](#), θ is given by $\theta_{\text{sep}} = \text{arccot}(\alpha)$.

The momentum [equations \(22\), \(23\)](#) can be rewritten as

$$(f + \zeta)\mathbf{u} = \mathbf{k} \times \nabla B, (26)$$

where B and ζ are defined by

$$B \doteq g'\eta + \frac{\nu^2}{2} \quad (27)$$

and

$$\zeta \doteq \nu_n. (28)$$

Substituting [\(26\)](#) into the steady-state mass continuity equation, it is straightforward to show that potential vorticity Q is conserved along streamlines. Thus, SG steady-state dynamics are described by [\(26\)](#) and by $\mathbf{u} \cdot \nabla Q = 0$, where

$$Q \doteq \frac{f + \zeta}{\eta - h}. \quad (29)$$

For unidirectional flow it is straightforward to show that Q can be written as a function of B . Here the problem will be simplified by considering Q to be constant. At each point, l , along the flow path, [Eqs. \(22\), \(28\), \(29\)](#) lead to an equation describing the across-stream structure of the interface height field:

$$g'\eta_{nn} - fQ\eta = -(f^2 + fhQ). (30)$$

Given Q and appropriate boundary conditions on η , (30) determines the across-stream structure of the current.

It is convenient to nondimensionalize the equations. An appropriate nondimensionalization can be found by taking η_0 as a vertical scale and L_{R0} as a horizontal scale. In nondimensional form, (30) becomes

$$\eta_{nn} = -1 + (\eta - h)Q, \quad (31)$$

and Q , B , and h become

$$Q = \frac{1 + \eta_{nn}}{h - \eta}, \quad (32)$$

$$B = \eta + \eta_n^2/2, \quad (33)$$

and

$$h = a(x^2 - \alpha^2 y^2), \quad \text{where } a \doteq g'A/f^2. \quad (34)$$

Given Q and appropriate boundary conditions (see below), (31) specifies the η field, provided that the topography is known as a function of n and l . In general, however, topography is given as a function of x and y so that the across-stream structure of the sill depends on the flow path. For elongated sills, this dependence is minimal; however, here we are interested in sills that are not necessarily elongated. Then, the effective topography can be quite different if, for example, the flow is assumed to be oriented along the separatrix, as opposed to the main axis of the sill.

The boundary conditions needed to integrate (31) are specified in one of two ways. The first of these allows for a mass of stagnant water (over which $\eta = 1$) to lie adjacent to the overflow current. At the boundary between the stagnant water and the overflow current, $\eta = 1$ and $\eta_n = 0$, corresponding to the requirements that the interface height field and velocity be continuous. This is the boundary condition used in K94. A second and more traditional boundary condition assumes the current to ground on both sides. On the left-hand side, where left is defined for an observer facing upstream, B is taken to be unity. Then, $\eta|_{\text{left}} = h|_{\text{left}}$ and $\eta_n|_{\text{left}}$ is given by (33), with $B = 1$. For both boundary conditions, the flow is assumed to be unidirectional, so profiles for which $\eta_n > 0$ over part of the domain were discarded. A shooting method was used to find the position of the left edge of the outflow that maximizes the flux.

b. Maximum transport over the sill

Here, we consider how the maximum flux across the sill depends on sill geometry, potential vorticity, the presence of a stagnant water mass, and the orientation of the flow path (e.g., whether the flow is parallel to the y axis or is along the separatrix isobath).

To begin, consider topography described by (6) with $\alpha = 1$, for which the length and width of the sill are comparable. Take the flow to be oriented along the y axis so that $\theta = 0$ in (24), (25) and $(n, l) = (x, y)$. The maximum allowable flux is constrained at $y = 0$ and is calculated using a shooting method. The results are shown in Fig. 4a for a range of the potential vorticities and sill widths. Also shown (Fig. 4b) is the difference in the maximum flux calculated by assuming each of the two boundary conditions on η . The stagnant water mass boundary condition gives a larger flux for wider sills. This occurs because the mean layer thickness in the current is larger in the stagnant water mass case, while the drop in the interface height field across the current is comparable to that found using the grounding boundary condition (Fig. 4c). For narrow sills, the grounding boundary condition allows for steeper slopes in the interface height field, as is evident from Fig. 4d. This, in turn, leads to larger velocities and higher transports.

Note also from Fig. 4a that the flux is relatively insensitive to the value of Q . This can be understood as follows. Potential vorticity affects the curvature of the η field through (31) and, since negative potential vorticities are not considered, the minimum value of η_{nn} is -1 . Thus, the increase in current speed (η_n) over its value at the left-hand side is bounded by the width of the sill. For narrow sills, if $\eta_n|_{\text{left}}$ is large compared to the nondimensional sill width, then η_n is essentially independent of Q . By extension, the velocity and transport have also become effectively independent of Q . For wider sills curvature in the η field affects the width of the current. This, however, does not appreciably affect the transport unless the current width becomes comparable to that of the sill. For relatively wide sills, the topography underlying the current is essentially flat so that the transport is insensitive to the current width.

The dependence of the across-sill flux T on Q is most pronounced for sills having characteristic widths close to unity. This is confirmed by Fig. 5, which shows $\partial \ln(T)/\partial Q$, giving a measure of the fractional change in T for small changes in Q . Transport is most sensitive to Q when the sill width L_{sill} is close to unity, where

$$L_{\text{sill}} \doteq a^{-1/2}. \quad (35)$$

An exception to this occurs for large potential vorticities, for which T remains sensitive to the choice of Q even for sills wide compared to the Rossby radius. The reason for this is that, for large Q , (31) gives that η_{nn} becomes positive wherever the layer thickness is too large. This tends to prohibit large velocities over the deeper portions of the sill, which restricts the net transport. Eventually the assumption of a unidirectional flow must be abandoned to get $O(1)$ transports. The role of bidirectional flow in obtaining $O(1)$ transports across wide sills when the grounding boundary condition is used was discussed by Killworth (Killworth 1992). The point emphasized here is that bidirectional flow is needed only in the limit of large potential vorticity, provided the stagnant water mass boundary condition is allowed.

Dependence of the maximum allowable transport on the sill width is most pronounced for narrow sills (see Fig. 4a). This dependence can be substantially weakened, however, when the angle at which the flow crosses the sill is allowed to vary. Figure 6 shows T as a function of θ for various choices of Q and for topography corresponding to the narrowest sill considered in Fig. 4 (i.e., to $L_{\text{sill}} = 0.25$). The angle θ is assumed to lie between 0 and θ_{sep} . Note that T increases with increasing θ and that the dependence of T on θ is much stronger than the dependence of T on Q . The reason for this is simply that the topographic cross section, $h(n)$, "seen" by the overflow is less restrictive with increasing θ .

An extreme example occurs when $\theta = \pi/4$, for which $T \rightarrow 1/2$. This results since, for $\theta = \pi/4$ and $\alpha = 1$, $n = (x - y)/(2)^{1/2}$ and $l = (x + y)/(2)^{1/2}$. Then, h can be written as $h = 2anl$. Thus, the n derivative of the topography vanishes identically at $l = 0$. In other words, the topography perpendicular to the presumed axis of the current is flat and therefore does not restrict the transport. This argument could be extended to an arbitrarily narrow sill. Obviously, however, it must be impossible to get an $O(1)$ transport through a very narrow sill. Therefore, one of our assumptions must break down for narrow sills. Presumably what happens is that the solutions just upstream and downstream of the sill become disaligned with one another. (The upstream and downstream solutions are described in the next section.) For the solutions to match, the current would then have to bend sharply in the vicinity of the sill. Once this happens, we are no longer justified in assuming the l and n length scales of the flow to be different. That is, the semigeostrophic approximation breaks down and the flow becomes fully nonlinear. Put another way, it is not clear that semigeostrophic dynamics can be used to estimate maximal fluxes through narrow sills that are not elongated. Given this, the transports calculated above (for $\theta = \theta_{\text{sep}}$) should be considered upper limits.

For more elongated sills (smaller α), θ_{sep} becomes small and the limit of traditional hydraulics is recovered. For narrow sills that are only moderately elongated, however, the maximum flux across the sill might depend significantly on θ . To see how elongated the sill must be before dependence on θ can be safely ignored, let us compare the dependence of T on θ to the dependence of T on Q . Take a measure of dependence on θ to be the difference in transport calculated assuming first $\theta = \theta_{\text{sep}}$ and then $\theta = 0$, for a fixed value of Q (say for $Q = 0$). (As discussed above, this should be considered to be an upper bound on the θ dependence.) Similarly, take a measure of dependence on Q to be the difference in transport calculated assuming small and large values of Q , for a fixed value of θ . The ratio of these,

$$\sigma \doteq \frac{T(Q = 0, \theta = \theta_{\text{sep}}) - T(Q = 0.95, \theta = \theta_{\text{sep}})}{T(Q = 0, \theta = \theta_{\text{sep}}) - T(Q = 0, \theta = 0)}, \quad (36)$$

then gives a measure of the relative importance of Q to that of θ in determining the maximum transport. (The high value of Q was chosen to be 0.95 instead of unity for technical reasons; the difference is minimal except for values of α very near 1.) Figure 7 shows σ plotted as a function of α for a narrow sill. For small values of α , dependence on Q is dominant. For sills that are only moderately elongated, however, the dependence of θ can be as or more important than the dependence on Q .

4. Conditions upstream and downstream of the sill

In this section, the nature of the flow upstream and downstream of the sill is considered. It is well known that the upstream solution for a basin filled to an ambient level of $\eta = 1$ corresponds to a flow positioned near the separatrix isobath. Above we have argued that this is imposed by the collapse of the PG problem. An example of the solution in the upstream basin is shown in Fig. 8a. Facing upstream, the ambient fluid lies to the left and the current grounds on the right. Fluid columns on the left-hand side of the current overlie topography deeper than the separatrix isobath, whereas columns on the

right overlies shallower topography. Downstream of the sill, the presence or absence of the stagnant water mass depends on the slope of the topography (see [Figs. 8b,c](#)). Also, downstream of the sill, columns on the right-hand side of the current overlie deeper topography, whereas columns on the left-hand side overlie shallower topography. Thus, somewhat curiously, fluid columns on the left-hand side of the current move uphill as they cross the sill, whereas columns on the right-hand side move downhill. This contrasts the traditional (e.g., rectangular cross section) solutions, for which all columns must move first uphill and then downhill as they cross the sill.

Downstream of the sill, the presence or absence of the stagnant water mass depends on the steepness of the topographic slope in the vicinity of the separatrix contour. Gentle slopes typically require the stagnant water mass, whereas steep slopes require the grounding boundary condition. Further steepening results in the position of the (grounding) solution moving downhill (not shown). This dependence of the presence of the stagnant water mass on the steepness of topography suggests the possibility of multiple solutions downstream of the sill. For example, when the slope varies strongly with distance from the separatrix isobath, there can be more than one current having the same Q , B , and T . [Figure 9](#) shows a case in which the topographic slope is taken to be gentle to the left and steep to the right, corresponding qualitatively to a shelf-slope topography. Here T and Q are taken to be 0.5 and 0, respectively. Two solutions exist, one corresponding to each of the possible boundary conditions on η .

Whether or not both solutions exist depends on the position of the break in the topographic slope, $n = n_0$. Referring to [Fig. 9](#), moving n_0 to the right will obviously not affect the stagnant water mass boundary solution. If n_0 is displaced too far to the right, however, the grounding solution ceases to exist since it becomes impossible to position a parabolic profile (corresponding to a zero potential vorticity current) such that a transport of one-half is obtained and the requirement that $B = 1$ on the left-hand side of the current is respected. Similarly, if n_0 is moved significantly to the left, it becomes impossible to find a solution corresponding to the stagnant water mass boundary condition that yields the assumed transport. Thus, by allowing n_0 to vary smoothly between these two extremes, one can construct a situation in which only one of the two solutions exists far upstream and only the other exists far downstream. This suggests the possibility that the solution may have to “jump” between two states similar to those shown in [Fig. 9](#). Depending on the sense in which n_0 varies with l , situations can be constructed for which either branch is the upstream branch.

The jump hypothesized above is distinct from that found by [Pratt \(1987\)](#). In his paper, the jump was described as being in the width of the current, rather than in the vertical position of the interface height field. The jump here, if it exists, would be in both the horizontal and vertical position of the current. Assuming the stagnant water solution to be the upstream branch, for example, the current would have to take a sharp turn downslope for the two solutions to match. Another difference between the situation described above and that described by Pratt is that, in his solutions (see, e.g., his [Fig. 4](#)), the upstream flow is downhill with the interface height field descending with a slope comparable to that of the topography. Here, the flow is essentially parallel to isobaths except at the hypothesized jump.

5. Summary

The focus of this work was on unforced flow over wide sills. The motivation for consideration of wide sills is that many deep ocean sills are wide with respect to the typically small abyssal Rossby radius. First, a simple f -plane PG model was developed and conditions on its validity were discussed. An initial value problem revealed that a field that initially respects these conditions can evolve into one that does not. In this sense, the f -plane PG dynamics are not appropriate for describing the steady-state flow. However, assuming that either friction or nonlinearities can arrest the breaking, the PG dynamics do predict various characteristics that the steady solution should exhibit. For example, they predict the path and transport of the flow and they suggest the presence of strong density gradients (or steep slopes in the interface height field) across the sill.

Since SG, rather than PG, dynamics are often used to describe flow over deep ocean sills, the question of whether the collapsing PG problem gives way to SG was discussed. It was found that this is not the case. Instead, the collapsing PG dynamics give way to an intermediate regime similar to that described by WY84 and by C86. Once this happens, it is not clear that the width of the current will continue to narrow. Thus, it is not obvious that SG dynamics are really appropriate to describing flow over wide sills.

It does seem reasonable, however, to expect that SG is appropriate to describing flow over sills that are narrow to moderately wide. Constant potential vorticity SG solutions were thus used to explore the dependence of the maximal mass transport across the sill on various factors. The most significant of these for sills wider than L_{R0} is whether or not one allows for a mass of stagnant water to lie adjacent to the overflow. That there may be such a water mass is suggested by analogy with the PG problem. Dependence of the transport on Q was rather weak and dependence on the sill width was only substantial for narrow sills. For narrow sills that are not elongated, it appears that curvature in the flow path is likely to become important. Once this happens, the semigeostrophic approximation can no longer be trusted. On a cautionary note, we should also add that the stability of these solutions was not considered.

Finally, several curiosities regarding the flow upstream and downstream of the sill were pointed out. First, it was noted that fluid columns crossing the sill typically move uphill on one side of the current and downhill on the other. Also, it was pointed out that for a shelf–slope topography there can sometimes be multiple equilibria. That is, there can be two solutions having the same potential vorticity, transport, and Bernoulli function.

Acknowledgments

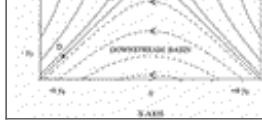
Helpful suggestions and comments from Peter Killworth, Tom Warn, and anonymous reviewers are gratefully acknowledged. This work was originally undertaken while the author was supported by a NERC grant awarded to Peter Killworth in Oxford. While in Canada, support was received from the following agencies: NSERC, DFO, AES and FCAR (Quebec).

REFERENCES

- Borenas, K. M., and P. A. Lundberg, 1986: Rotating hydraulics of flow in a parabolic channel. *J. Fluid Mech.*, **167**, 309–326..
- Cushman-Roisin, B., 1986: Frontal geostrophic dynamics. *J. Phys. Oceanogr.*, **16**, 132–143..
- Dalziel, S. B., 1992: Maximal exchange in channels with nonrectangular cross sections. *J. Phys. Oceanogr.*, **22**, 1188–1206..
- Gill, A. E., 1976: Adjustment under gravity in a rotating channel. *J. Fluid Mech.*, **77**, 603–621..
- , 1977: The hydraulics of rotating-channel flow. *J. Fluid Mech.*, **80**, 641–671..
- , M. K. Davey, E. R. Johnson, and P. F. Linden, 1986: Rossby adjustment over a step. *J. Mar. Res.*, **44**, 713–738..
- Johnson, E. R., 1985: Topographic waves and the evolution of coastal currents. *J. Fluid Mech.*, **160**, 499–509..
- Killworth, P. D., 1992: Flow properties in rotating stratified hydraulics. *J. Phys. Oceanogr.*, **22**, 997–1017..
- , 1994: On reduced gravity flow through sills. *Geophys. Astrophys. Fluid Dyn.*, **75**, 91–106..
- Pratt, L. J., 1987: Rotating shocks in a separated laboratory channel flow. *J. Phys. Oceanogr.*, **17**, 483–491..
- , and L. Armi, 1990: Two layer rotating hydraulics: Strangulation, remote and virtual controls. *Pure Appl. Geophys.*, **133**, 587–617..
- , and P. A. Lundberg, 1991: Hydraulics of rotating strait and sill flow. *Annu. Rev. Fluid Mech.*, **23**, 81–106..
- Salmon, R., 1995: A simple model of abyssal flows. *Topographic Effects in the Ocean: Proceedings of the 'Aha Huliko'a Hawaiian Winter Workshop*, P. Müller and D. Henderson, Eds., SOEST Special Publications, 157–161..
- Stern, M. E., 1972: Hydraulically critical rotating flow. *Phys. Fluids*, **15**, 2062–2064..
- Whitehead, J. A., 1989: Internal hydraulic control in rotating fluids—applications to oceans. *Geophys. Astrophys. Fluid Dyn.*, **48**, 169–192..
- , 1995: Critical control by topography—Deep passages, straits and shelf fronts. *Topographic Effects in the Ocean: Proceedings of the 'Aha Huliko'a Hawaiian Winter Workshop*, P. Müller and D. Henderson, Eds., SOEST Special Publications, 141–156..
- , A. Leetma, and R. A. Knox, 1974. Rotating hydraulics of strait and sill flows. *Geophys. Fluid Dyn.*, **6**, 101–125..
- Williams, G. P., and T. Yamagata, 1984: Geostrophic eddies, intermediate solitary vortices and Jovian eddies. *J. Atmos. Sci.*, **41**, 453–478..
[Find this article online](#)

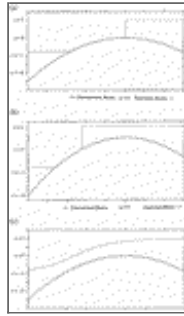
Figures





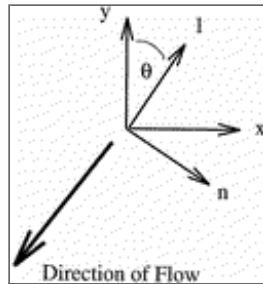
[Click on thumbnail for full-sized image.](#)

Fig. 1. Plan view of topography in the vicinity of the sill. Arrows on the isobaths indicate the sense of the characteristic velocity, c . The points A, B, C, and D are referred to in the text. The PG solution collapses into a thin current lying along the line containing points C and D.



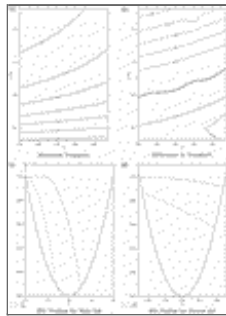
[Click on thumbnail for full-sized image.](#)

Fig. 2. Comparison of the long time PG solution with a schematic depicting the case of controlled flow over a sill for the nonrotating case. Shown are y - z sections of the interface height fields and topography. (a) The long time PG solution for a section containing the saddle. (b) Similar to (a) except at an x position to the left of the saddle (i.e., $x < 0$). (c) Schematic depicting a nonrotating hydraulically controlled case. Note that the PG solutions and the control case are similar in that they both show sharp gradients in the interface height field across the sill. Allowing for bottom friction would have the effect of smoothing out the discontinuity in the PG case, which would further increase this resemblance.



[Click on thumbnail for full-sized image.](#)

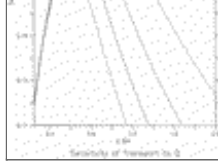
Fig. 3. Relationship of the (n, l) and the (x, y) coordinate systems.



[Click on thumbnail for full-sized image.](#)

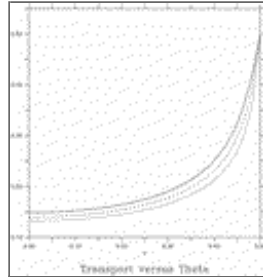
Fig. 4. (a) Maximum flux over sill for a range of Q and sill widths. Here the flow is assumed to be oriented along the y axis; L_{sill} is defined as the (nondimensional) half-width of the sill at a height of $z = 1$. (b) The difference in maximum transport calculated by assuming the flow to ground on both sides of the sill versus assuming a stagnant water mass to lie adjacent to the flow. Negative values correspond to situations in which the stagnant water mass boundary condition yields higher fluxes. (c) Interface height field profiles corresponding to the maximum transport for the two boundary conditions for a relatively wide sill. (d) As in (c), but for a narrow sill.





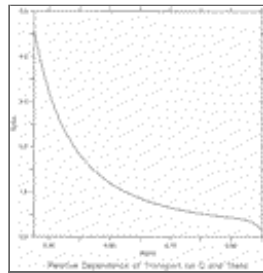
Click on thumbnail for full-sized image.

Fig. 5. Sensitivity of the flux to small changes in Q , calculated as $\frac{d}{dQ} \ln(T)$ and plotted against L_{sill} . The curves correspond to $Q = 0.1, 0.3, 0.5, 0.7,$ and 0.9 , respectively (bottom to top). Other parameters are as in Fig. 4. The dependence of the flux over the sill on Q is most pronounced for sills having characteristic widths on the order of the Rossby radius. An exception to this is for wider sills and large potential vorticities, for which T remains relatively sensitive to the choice of Q .



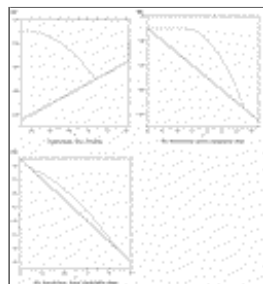
Click on thumbnail for full-sized image.

Fig. 6. Plot of T versus θ for $L_{\text{sill}} = 0.25$ and $\alpha = 1$. The horizontal (θ) axis is scaled by a factor of π . The top, middle, and bottom curves correspond to $Q = 0, Q = 0.5,$ and $Q = 0.99$, respectively. Note that the dependence of T on θ is much stronger than the dependence of T on Q . Note also that $T \rightarrow 1/2$ as $\theta \rightarrow \pi/2$.



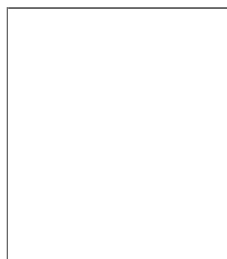
Click on thumbnail for full-sized image.

Fig. 7. Relative dependence of T on Q to that of T on θ for a narrow sill ($L_{\text{sill}} = 0.25$). Plotted is the ratio σ as a function of α . Small values indicate that T depends more strongly on θ than on Q . For small values of α (elongated sills) dependence of transport on Q is more important of the two, and the classic limit of rotating hydraulics is recovered.



Click on thumbnail for full-sized image.

Fig. 8. (a) Typical profile of the solution far upstream. (b) Typical profile of the solution far downstream, for the case of gentle topography. (c) Typical profile of the solution far downstream, for the case of steep topography. Note that a streamline for which $B \approx 1$ overlies topography deeper than the sill upstream and more shallow than the sill downstream.





Click on thumbnail for full-sized image.

Fig. 9. An example of multiple solutions over a topography for which the slope increases in magnitude with depth. Both η profiles correspond to a current having $Q = 0$ and $T = 1/2$. The point at which the slope changes corresponds to $n = n_0$.

* Current affiliation: Le Centre de Recherche en Calcul Appliqué à Montréal, Montreal, Quebec, Canada.

Corresponding author address: Dr. David N. Straub, Atmospheric and Oceanic Sciences, McGill University, 805 Sherbrooke O., Montreal, Quebec, PQ H3A 2K6, Canada.

E-mail: david@gumbo.meteo.mcgill.ca

top ▲



© 2008 American Meteorological Society [Privacy Policy and Disclaimer](#)
Headquarters: 45 Beacon Street Boston, MA 02108-3693
DC Office: 1120 G Street, NW, Suite 800 Washington DC, 20005-3826
amsinfo@ametsoc.org Phone: 617-227-2425 Fax: 617-742-8718
[Allen Press, Inc.](#) assists in the online publication of *AMS* journals.